

Effect of continuum couplings in fusion of halo ^{11}Be on ^{208}Pb around the Coulomb barrier

A. Diaz-Torres^{*} and I.J. Thompson

Physics Department, University of Surrey, Guildford GU2 7XH, United Kingdom

(October 27, 2018)

The effect of continuum couplings in the fusion of the halo nucleus ^{11}Be on ^{208}Pb around the Coulomb barrier is studied using a three-body model within a coupled discretised continuum channels (CDCC) formalism. We investigate in particular the role of continuum-continuum couplings. These are found to hinder total, complete and incomplete fusion processes. Couplings to the projectile $1p_{1/2}$ bound excited state redistribute the complete and incomplete fusion cross sections, but the total fusion cross section remains nearly constant. Results show that continuum-continuum couplings enhance the irreversibility of breakup and reduce the flux that penetrates the Coulomb barrier. Converged total fusion cross sections agree with the experimental ones for energies around the Coulomb barrier, but underestimate those for energies well above the Coulomb barrier.

Introduction: The existence and the role of the breakup process of weakly bound projectiles in complete fusion and scattering mechanisms have been extensively investigated in recent years both theoretically [1–6] and experimentally [7–16], but there is not yet any definitive conclusion. There are contradictory theoretical works which predict either the suppression [1–4] or the enhancement [5] of the complete fusion cross section due to the coupling of the relative motion of the nuclei to the breakup channel.

Recent coupled channels calculations for $^{11}\text{Be}+^{208}\text{Pb}$ [6] have shown that the coupling of the relative motion to the breakup channel has two effects, depending on the value of the bombarding energy, namely (i) a reduction of the complete fusion cross sections at energies above the Coulomb barrier due to the loss of incident flux, and (ii) an enhancement of the complete fusion cross sections at energies below the Coulomb barrier due to the dynamical renormalisation of the nucleus-nucleus potential. Using the isocentrifugal approximation and an incoming boundary condition inside the barrier, this calculation did not include the effect of the projectile’s halo structure on the monopole projectile-target potential. Nor did it include the excitation to partial waves other than $p_{3/2}$ in the continuum, or the continuum-continuum and bound excited states couplings in either reaction partner. Moreover, only a small interval of energy for continuum states (up to 2 MeV) was considered.

The couplings between continuum states have been shown to be crucial to understand the breakup of ^8B on a ^{58}Ni target at low energy $E_{lab} = 25.8$ MeV [19,20]. Therefore, it could be expected that continuum-continuum couplings significantly affect the role of breakup process in fusion of halo nuclei around the Coulomb barrier. We believe that

^{*}E-mail: A.Diaz-Torres@surrey.ac.uk

continuum-continuum couplings enhance the irreversibility of the breakup process (thus once the projectile gets dissociated, it will find it very hard to find its way back to the bound states). Thus, the continuum-continuum couplings are expected to reduce the flux in bound projectile channels and, therefore, should inhibit (at least) the complete fusion. We expect that, with an increasing breakup subspace, governed by both the maximum energy and continuum partial waves, continuum-continuum couplings will reduce the fusion cross sections until convergence is reached.

The aim of this paper is to clarify the role of these continuum couplings on the fusion of the halo projectile ^{11}Be on a ^{208}Pb target at energies around the Coulomb barrier. Calculations are carried out using a three-body model [19,20] in the framework of the CDCC formalism [21,22]. Full coupled channels calculations are performed with the code FRESKO [23].

In calculation of fusion cross sections, we simultaneously include (i) the effect of the projectile's halo structure on the projectile-target potential, (ii) both the transition to its bound excited state and its dissociation caused by inelastic excitations to different partial waves in the continuum, induced by the projectile fragments-target interactions (coulomb + nuclear), and (iii) couplings (bound-continuum and continuum-continuum) between its excited states. We do not include transfer or inelastic channels of the target. Fusion cross sections for projectile bound channels and for projectile breakup channels will be defined in terms of a short-ranged imaginary bare potential defined in the center of mass coordinate of the projectile in conjunction with channel dependent wave functions for the projectile-target radial motion.

Model: In the $^{11}\text{Be} + ^{208}\text{Pb}$ reaction, the three-bodies involved are the ^{10}Be core (C), the valence (halo) neutron (v), and the ^{208}Pb target (T).

Let \vec{R} be the coordinate from the target to the center of mass of the projectile, and \vec{r} the internal coordinate of the projectile. The position coordinates of the projectile fragments with respect to the target are $\vec{r}_{vT} = \vec{R} + \frac{A_P-1}{A_P}\vec{r}$ and $\vec{R}_{CT} = \vec{R} - \frac{1}{A_P}\vec{r}$, where A_P is the mass of the projectile.

The dynamics of the three-bodies is described by the Schrödinger equation in the over-all centre of mass system. The two-body potentials V_{CT} , V_{vT} and V_{vC} depend only on relative coordinates indicated as their arguments and do not excite the internal degrees of freedom of the core and the target nucleus. Following [6], these potentials are considered as real, but in addition we use for fusion a bare short-ranged (well inside the Coulomb barrier) imaginary central potential $iW_F(R)$ defined in the center of mass of the projectile for the projectile-target radial motion. The use of this short-ranged imaginary potential is equivalent to the use of an incoming boundary condition inside the Coulomb barrier to study fusion [17,18].

In order to describe the breakup of a projectile such as ^{11}Be , we consider the inelastic excitations induced by V_{CT} , V_{vT} in the $n + ^{10}\text{Be}$ system from the ground state $\phi_{(ls)j,n}^{g,s}(r)$ to excited states in the continuum $u_{(ls)j,k}(r)$, for some wave-number k and partial wave l , and also couplings between all such continuum states. The use of such single energy eigenstates, however, would result in calculations of form factors for continuum-continuum couplings which do not converge, as the continuum wave functions are not square integrable. The CDCC method [21,22] is used to obtain square integrable continuum bins states $\phi_{(ls)j,[k_1,k_2]}(r)$ averaged over a narrow range of wave-numbers $[k_1, k_2]$. We label these bin states by their wave-number limits $[k_1, k_2]$ and their angular momentum quantum numbers $(ls)j$. The

bound states of the projectile $\phi_{(ls)j,n}(r)$ and the single energy scattering wave functions $u_{(ls)j,k}(r)$ which form the continuum bins $\phi_{(ls)j,[k_1,k_2]}(r)$, are obtained by solving a Schrödinger equation with the potential V_{vC}^l which may be l -dependent. The bin wave functions are defined as

$$\phi_{(ls)j,[k_1,k_2]}(r) = \sqrt{\frac{2}{\pi N}} \int_{k_1}^{k_2} w(k) e^{-i\delta_k} u_{(ls)j,k}(r) dk, \quad (1)$$

where δ_k is the scattering phase shift for $u_{(ls)j,k}(r)$. The normalisation constant is $N = \int_{k_1}^{k_2} |w(k)|^2 dk$ for the assumed weight function $w(k)$, here taken to be either unity for non- s -wave bins or k for s -wave bins. These bin states are normalised $\langle \phi | \phi \rangle = 1$ once a sufficiently large maximum radius r_{bin} for r is taken. They are orthogonal to any bound states, and are orthogonal to other bin states if their energy ranges do not overlap. The phase factor $e^{-i\delta_k}$ ensures that they are real valued for real potentials V_{vC}^l .

The radial wave functions $f_{\alpha J}(R)$ for the projectile-target relative motion satisfy the set of coupled equations [19]

$$\begin{aligned} & \left[-\frac{\hbar^2}{2\mu} \left(\frac{d^2}{dR^2} - \frac{L(L+1)}{R^2} \right) + V_{\alpha:\alpha}^J(R) + iW_F(R) + \epsilon_\alpha - E \right] f_{\alpha J}(R) \\ & = \sum_{\alpha' \neq \alpha} i^{L'-L} V_{\alpha:\alpha'}^J(R) f_{\alpha' J}(R), \end{aligned} \quad (2)$$

where μ , L , J , E and α ($\{L, l, s, j, n$ or $[k_1, k_2]\}$) denote the projectile-target reduced mass, the projectile orbital angular momentum, the total angular momentum, the total energy, and the set of quantum numbers, respectively. For unbound states of the projectile, ϵ_α is the mean energy of continuum bin $[k_1, k_2]$, or $\epsilon_\alpha < 0$ for bound states. $V_{\alpha:\alpha'}^J$ describes the coupling between the different internal states $\phi_\alpha(\vec{r})$ of the projectile

$$V_{\alpha:\alpha'}^J(\vec{R}) = \langle \phi_\alpha(\vec{r}) | V_{CT}(\vec{R}_{CT}) + V_{vT}(\vec{r}_{vT}) | \phi_{\alpha'}(\vec{r}) \rangle. \quad (3)$$

Assuming that the potentials V_{CT} and V_{vT} are central, the Legendre multipole potentials can be formed as

$$\Lambda_K(R, r) = \frac{1}{2} \int_{-1}^{+1} [V_{CT}(\vec{R}_{CT}) + V_{vT}(\vec{r}_{vT})] P_K(x) dx, \quad (4)$$

where K is the multipole and $x = \hat{r} \cdot \hat{R}$ is the cosine of the angle between \vec{r} and \vec{R} . Since the spin s of the neutron is fixed, the coupling form factor (3) between states $\phi_{\alpha'}(r)$ and $\phi_\alpha(r)$ is

$$\begin{aligned} V_{\alpha:\alpha'}^J(R) &= \sum_K (-1)^{j+j'-J-s} \hat{j} \hat{j}' \hat{l} \hat{l}' \hat{L} \hat{L}' (2K+1) W(jj' ll'; Ks) W(jj' LL'; KJ) \\ &\times \begin{pmatrix} K & l & l' \\ 0 & 0 & 0 \end{pmatrix} \begin{pmatrix} K & L & L' \\ 0 & 0 & 0 \end{pmatrix} \int_0^\infty \phi_\alpha(r) \Lambda_K(R, r) \phi_{\alpha'}(r) dr. \end{aligned} \quad (5)$$

Eqs. (2) are solved with the usual scattering boundary conditions [23].

The total fusion cross section σ_{tot} is defined in terms of that amount of flux which leaves the coupled channels set because of the short-ranged imaginary potential $iW_F(R)$.

Since complete fusion is a process where all the nucleons of the projectile are captured by the target nucleus and following [6], we define in our model the complete fusion cross section as the absorption cross section from projectile bound channels (complete fusion from both ground state (elastic) and bound excited state)

$$\sigma_{CF} = \frac{\pi}{2\mu E} \sum_J (2J+1) P_J, \quad (6)$$

where E is the bombarding energy and P_J is the complete fusion probability for the partial wave J . The complete fusion probability P_J is [24]

$$P_J = \frac{8}{\hbar(2E/\mu)^{1/2}} \sum_{\alpha (\epsilon_\alpha < 0)} \int_0^\infty |f_{\alpha J}(R)|^2 (-W_F(R)) dR. \quad (7)$$

The complete fusion cross section (6)-(7) represents a lower limit for the physical complete fusion cross section, since we have assumed no capture of all projectile fragments (^{10}Be and the halo neutron) from breakup channels. In reality, these events should contribute to the complete fusion, but cannot be distinguished in our model from the capture of only one projectile fragment.

The incomplete fusion σ_{ICF} (fusion of ^{10}Be) is then defined as the absorption from breakup channels

Results and discussion: The experimental spectrum of ^{11}Be exhibits a $1/2^+$ ground state and a single, $1/2^-$, bound excited state with energies of -0.50 MeV and -0.18 MeV, respectively. In a pure single-particle picture, the ground and the bound excited states of ^{11}Be have $2s_{1/2}$ and $1p_{1/2}$ single-particle configurations, respectively. These configurations can be associated with single-particle states generated by different V_{vC}^l Woods-Saxon potentials [25] including a spin-orbit term. For the $2s_{1/2}$ state, we use a Woods-Saxon potential with parameters $V_0 = -51.51$ MeV, $r_0 = 1.39$ fm and $a = 0.52$ fm. For the $1p_{1/2}$ state, we use a Woods-Saxon potential including a spin-orbit term, similar to that used in [25], with the same geometry, i.e. $V_0 = -30$ MeV, $r_0 = 1.39$ fm, $a = 0.52$ fm and $V_0^{s.o.} = 4.39$ MeV.

First, we study qualitatively the effect of continuum couplings on fusion cross sections by using a reduced breakup subspace with regard to the maximum energy of the projectile continuum states. A continuum breakup subspace with partial waves $s_{1/2}$, $p_{1/2}$, $p_{3/2}$, $d_{3/2}$ and $d_{5/2}$, for the halo neutron- ^{10}Be core relative motion, is used. For each partial wave, the continuum subspace is discretised in 6 bins which are equally spaced in wave-number k , up to a maximum wave-number $k_{max} = 0.3612 \text{ fm}^{-1}$ (a maximum energy of 3 MeV), with a step of $\Delta k = 0.0602 \text{ fm}^{-1}$. In Fig.1, we illustrate the continuum discretisation used to define the energy bins included in these calculations. The calculation is thus performed with 30 excited continuum channels. The s - and p -wave continuum states have been consistently generated by the same potential V_{vC}^l as that of the bound state of the same angular momentum l . The d -wave continuum states have been generated by the same potential as that of the p -waves.

In the present work, Woods-Saxon parametrisations given in [26] and in [27] are used for the nuclear part of the potentials V_{CT} ($V_0 = -46.764$ MeV, $r_0 = 1.192$ fm and $a = 0.63$ fm)

and V_{vT} ($V_0 = -44.019$ MeV, $r_0 = 1.27$ fm and $a = 0.67$ fm), respectively. A short-ranged Woods-Saxon potential W_F with parameters $V_0 = -50$ MeV, $r_0 = 1$ fm and $a = 0.1$ fm is used for the fusion potential. The results depend only weakly on the geometry of this potential, as long as it is well inside the Coulomb barrier and strong enough that the mean-free path of the projectile inside the barrier is much smaller than the dimensions of W_F . The fusion cross sections for $V_0 = -50$ MeV are those for $V_0 = -10$ MeV changed by $\sim 1\%$.

Since we are interested in fusion cross sections, partial waves for the projectile-target relative motion up to only $L_{max} = 50$ (partial-wave total fusion cross section $\sim 10^{-3}$ mb) are included. Our calculations include monopole, dipole and quadrupole contributions ($K=0,1$ and 2) of the potentials V_{CT} and V_{vT} for both nuclear and Coulomb parts. The couplings $V_{\alpha:\alpha'}^J(R)$ are taken into account up to a projectile-target radial distance $R_{coup} = 100$ fm. To calculate both the continuum bins (1) and couplings $V_{\alpha:\alpha'}^J(R)$ (5), which include these bins, radii $r \leq r_{bin} = 100$ fm are used.

Figs.2a and 2b show fusion cross sections as a function of the bombarding energy in the center of mass system. For comparison, we present cross sections in the absence of couplings (thin solid curve). In Fig.2a, calculations include transitions from and to the projectile bound states, but do not include continuum-continuum couplings. In this case, we found that the effect of the projectile bound excited state $1p_{1/2}$ on the total, complete and incomplete fusion cross sections is quite weak ($\sim 10\%$). The couplings to the bound excited state $1p_{1/2}$ only redistributes the complete fusion cross section (thick solid curve) between the elastic channel and this channel, the fusion contribution from the elastic channel being $1.7 - 3.4$ times larger than from the bound excited state $1p_{1/2}$ for the range of energies studied. We would like to note that these fusion excitation functions show similar trends as those obtained by Hagino et al. [6]. We agree that complete fusion cross sections are strongly enhanced due to the couplings to the projectile excited states compared with the no-coupling case at energies below and just above the Coulomb barrier ($V_B \approx 36$ MeV for the elastic channel), whereas they are hindered at above barrier energies.

In Fig.2b, we show the effect of continuum-continuum couplings on the total and complete fusion cross sections of Fig. 2a. It is found that well above the Coulomb barrier, both total and complete fusion cross sections are suppressed compared with the no-coupling case, and enhanced well below the barrier. Just below the Coulomb barrier ($34 \text{ MeV} \leq E_{c.m.} \leq 36 \text{ MeV}$), complete fusion cross sections are suppressed, but this is not the case for total fusion cross sections. In the present case, we found that couplings to the projectile bound excited state $1p_{1/2}$ redistribute (dot-dashed curve) the complete and incomplete fusion cross sections, while the total fusion cross sections (dashed curve) remain nearly constant. With couplings to the bound excited state $1p_{1/2}$, the contribution to complete fusion from the elastic channel is similar to the one from the bound excited state $1p_{1/2}$ for energies below the Coulomb barrier, and $1.7 - 8$ times smaller for energies above the Coulomb barrier.

Fig.3 shows incomplete fusion excitation functions (difference between the total and the complete fusion curves) for both cases presented above, namely in Figs.2a and 2b. We can observe that continuum-continuum couplings significantly reduce the incomplete fusion cross sections (dashed curve). The case when the couplings to the bound excited state $1p_{1/2}$ are not included is shown by the dot-dashed curve.

From Fig.2b and Fig.3, it is observed that continuum-continuum couplings strongly affect the predicted total, complete and incomplete fusion cross sections. This implies that the

fusion dynamics strongly depends on continuum-continuum couplings. Since the short-ranged imaginary potential is well confined within the Coulomb barrier, we deduce that continuum-continuum couplings mainly reduce the flux that penetrates the barrier, while couplings to the projectile bound excited state $1p_{1/2}$ mainly redistribute, among the complete and incomplete fusion channels, the flux that has already penetrated the Coulomb barrier.

We have checked the convergence of reported fusion cross sections (total, complete and incomplete) with the size of the breakup subspace, and have found the following when couplings between all projectile excited states (bound-continuum and continuum-continuum) are included in the calculation:

- The maximum energy of the continuum states (Fig.4): a maximum energy beyond 9 MeV is needed to obtain converged results. With respect to the fusion cross sections for a maximum energy of 9 MeV (dashed curve), fusion cross sections for a maximum energy of 10 MeV (full squares) are changed by $\sim 10\%$ for energies around the Coulomb barrier. For energies well above the barrier, fusion cross sections are changed by $\sim 1.5\%$.
- The density of the continuum discretisation (Fig.5): a density greater than 1.67 bins/MeV is needed to obtain converged results. The same density is used for all partial waves in the continuum. With respect to fusion cross sections for a density of 1.67 bins/MeV (dotted curve), fusion cross sections for a density of 2 bins/MeV (dashed curve) are changed by $\sim 6.5\%$ for energies around the Coulomb barrier. For energies well above the barrier, fusion cross sections are changed by $\sim 1.6\%$.
- The number of partial waves in the continuum and potential multipoles (Fig.6): partial waves beyond $f_{5/2}$, $f_{7/2}$ and potential multipoles beyond the octupole contribution ($K=3$) are needed to obtain converged results. With respect to fusion cross sections for continuum partial waves up to f -waves and potential multipoles $K \leq 3$ (full circles), fusion cross sections for continuum partial waves up to g -waves and potential multipoles $K \leq 4$ (full triangles) are changed by $\sim 8\%$ (total fusion), $\sim 100\%$ (complete fusion) and $\sim 3\%$ (incomplete fusion), respectively, for energies around the Coulomb barrier. For energies well above the barrier, fusion cross sections are changed by $\sim 13\%$. The calculation including both continuum partial waves up to g -waves and potential multipoles $K \leq 4$ (full triangles) is presently at the limit of our computational capability.

Fig.7 shows experimental total fusion cross sections (full squares) for the similar system $^{11}\text{Be} + ^{209}\text{Bi}$ [10], which should not differ too much from the reaction studied. By comparing converged total fusion cross sections for $^{11}\text{Be} + ^{208}\text{Pb}$ (full stars), calculated within our model, with the experimental ones for $^{11}\text{Be} + ^{209}\text{Bi}$, it is observed that the converged total fusion excitation function does not reproduce the experimental one. They do agree with the experiment for energies around the Coulomb barrier, but underestimate the data by $\sim 41\%$ for energies well above the Coulomb barrier.

A crude estimation of the effect of target excitations on the total fusion cross section has been done by (i) fitting the converged total fusion cross section in a single (elastic) channel calculation by finding an appropriate projectile-target real Wood-Saxon potential with an energy dependent depth and the geometry $r_0 = 1.179$ fm and $a = 0.658$ fm, and

then (ii) including the target excitations as in ref. [29]. Such estimation reveals that the effect is quite weak. Fusion cross sections are increased ~ 1.28 times for energies around the Coulomb barrier, while they remain nearly constant for energies well above the Coulomb barrier.

The experimental cross sections for $^{11}\text{Be} + ^{209}\text{Bi}$ were obtained [10] as the sum of three channels: $5n+4n+\text{fission}$. It was pointed out in ref. [28] that the $3n$ channel, expected to be relevant below the barrier, could not be measured and at the same time the fission cross section could have been overestimated. A new experiment is necessary in order to clarify the ^{11}Be fusion mechanism discussed in the present work.

Summary and conclusions: Fusion cross sections calculated in the CDCC framework depend strongly on continuum-continuum couplings. We do not include transfer or inelastic channels of the target. Continuum-continuum couplings hinder total, complete and incomplete fusion processes. Couplings to the projectile $1p_{1/2}$ bound excited state redistribute the complete and incomplete fusion cross sections, but do not change the total fusion cross section. Results show that continuum-continuum couplings enhance the irreversibility of breakup and reduce the flux that penetrates the Coulomb barrier. A large breakup subspace is needed to obtain converged fusion cross sections. The converged total fusion excitation function does not reproduce the experimental one: converged total fusion cross sections agree with the experimental ones for energies around the Coulomb barrier, but underestimate those for energies well above the Coulomb barrier. A crude estimation of the effect of target excitations on the total fusion cross section reveals that it is quite weak. A new experiment seems to be necessary to clarify the ^{11}Be fusion mechanism discussed in the present work. The total fusion cross section is unambiguously calculated in our formalism, but this is not the case for the complete fusion since the capture of all projectile fragments from breakup channels cannot always be distinguished from the capture of only one projectile fragment.

Acknowledgments

We thank Prof. Jeff Tostevin for a careful reading of the paper, helpful discussions and comments. We also thank Profs. Cosimo Signorini and Andrea Vitturi for fruitful discussions. We are grateful to Dr. Atsushi Yoshida for the experimental data. UK support from the EPSRC grant GR/M/82141 is acknowledged.

-
- [1] M.S. Hussein, M.P. Pato, L.F. Canto and R. Donangelo, Phys. Rev. C 46, 377 (1992); Phys. Rev. C 47, 2398 (1993).
 - [2] L.F. Canto, R. Donangelo, P. Lotti and M.S. Hussein, Phys. Rev. C 52, R2848 (1995).
 - [3] N. Takigawa, M. Kuratani and H. Sagawa, Phys. Rev. C 47, R2470 (1993).
 - [4] K. Yabana, Prog. Theor. Phys. 97, 437 (1997).
 - [5] C.H. Dasso and A. Vitturi, Phys. Rev. C 50, R12 (1994).
 - [6] K. Hagino, A. Vitturi, C.H. Dasso and S.M. Lenzi, Phys. Rev. C 61, 037602 (2000).
 - [7] A. Yoshida et al., Phys. Lett. B 389, 457 (1996).
 - [8] J. Takahashi et al., Phys. Rev. Lett. 78, 30 (1997).
 - [9] K.E. Rehm et al., Phys. Rev. Lett. 81, 3341 (1998).

- [10] C. Signorini et al., Eur. Phys. J. A 2, 227 (1998); Eur. Phys. J. A 5, 7 (1999).
- [11] J.J. Kolata et al., Phys. Rev. Lett. 81, 4580 (1998).
- [12] M. Dasgupta et al., Phys. Rev. Lett. 82, 1395 (1999).
- [13] M. Trotta et al., Phys. Rev. Lett. 84, 2342 (2000).
- [14] E.F. Aguilera et al., Phys. Rev. Lett. 84, 5058 (2000).
- [15] C. Signorini et al., Phys. Rev. C 61, 061603 (2000).
- [16] S. B. Moraes et al., Phys. Rev. C 61, 064608 (2000).
- [17] M.J. Rhoades-Brown and P. Braun-Munzinger, Phys. Lett. B 136, 19 (1984).
- [18] S. Landowne and S.C. Pieper, Phys. Rev. C 29, 1352 (1984).
- [19] F.M. Nunes and I.J. Thompson, Phys. Rev. C 59, 2652 (1999).
- [20] J.A. Tostevin, F.M. Nunes and I.J. Thompson, Phys. Rev. C 63, 024617 (2001).
- [21] M. Kawai, Prog. Theor. Phys. Suppl. 89, 11 (1986).
- [22] N. Austern, Y. Iseri, M. Kamimura, M. Kawai, G. Rawitscher and M. Yahiro, Phys. Rep. 154, 125 (1987).
- [23] I.J. Thompson, Comput. Phys. Rep. 7, 167 (1988); FRESCO users' manual (version FRXX.09g), University of Surrey, United Kingdom (unpublished).
- [24] G.R. Satchler, M.A. Nagarajan, J.S. Lilley and I.J. Thompson, Ann. Phys. (N.Y.) 178, 110 (1987).
- [25] C.H. Dasso, S.M. Lenzi and A. Vitturi, Phys. Rev. C 59, 539 (1999).
- [26] R.A. Broglia and A. Winther, in *Heavy-Ion Reactions (Parts I and II FIP Lecture Notes Series)*, (Addison-Wesley, New York 1991).
- [27] A. Bohr and B. Mottelson, in *Nuclear Structure*, (Benjamin, New York 1969).
- [28] C. Signorini, in *Proceedings RIB00 International Conference*, Hayama, Japan, November 2000, eds. T. Nakamura et al., to be published in a special issue of Eur. Phys. J. A.
- [29] I.J. Thompson, M.A. Nagarajan, J.S. Lilley and M.J. Smithson, Nucl. Phys. A 505, 84 (1989).

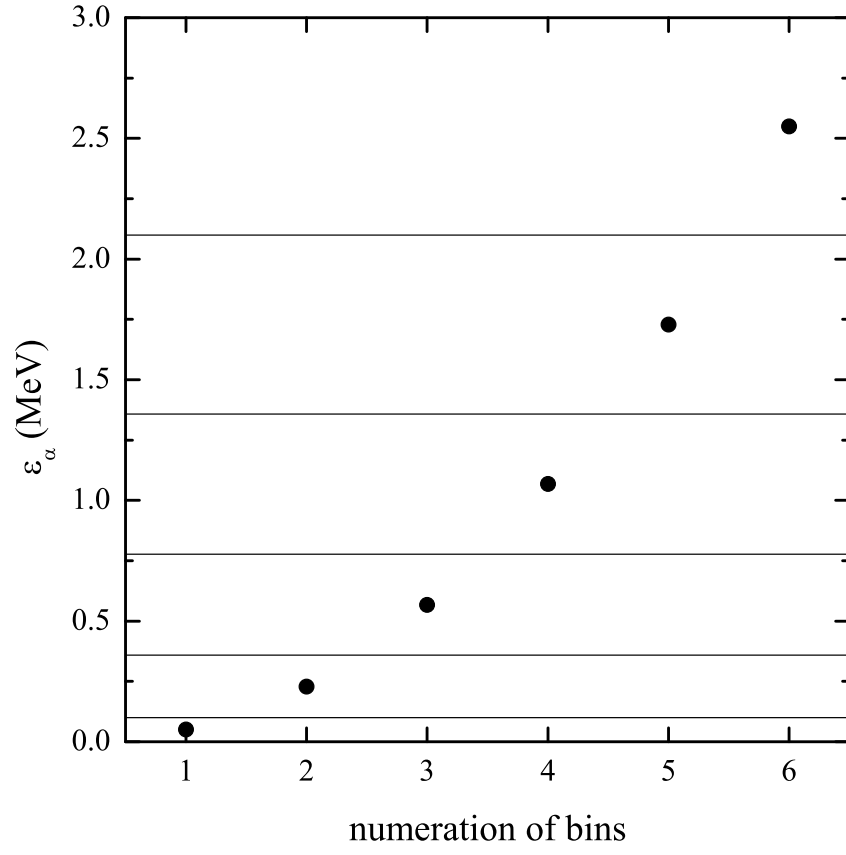


FIG. 1. Continuum discretisation used to define the energy bins. The central energies of bins are shown by full circles.

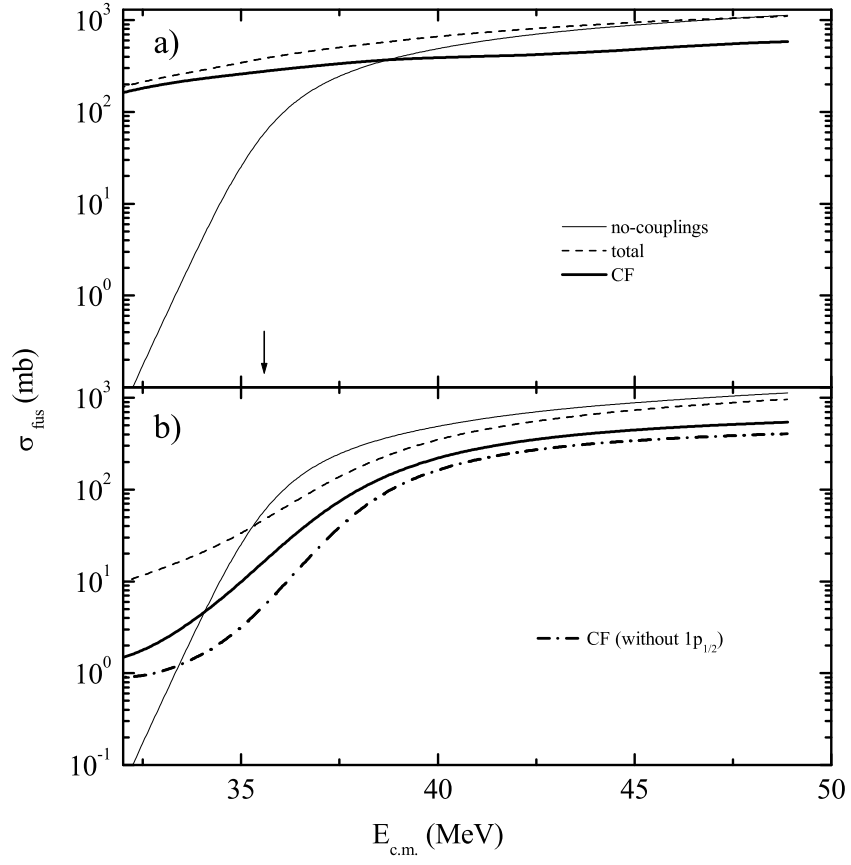


FIG. 2. Fusion cross sections as a function of the bombarding energy in the center of mass system for $^{11}\text{Be} + ^{208}\text{Pb}$. a) Include only couplings from and to the ^{11}Be bound states. b) Couplings between all ^{11}Be excited states (continuum-continuum) are included. See text for further details. The arrow indicates the Coulomb barrier for the elastic channel.

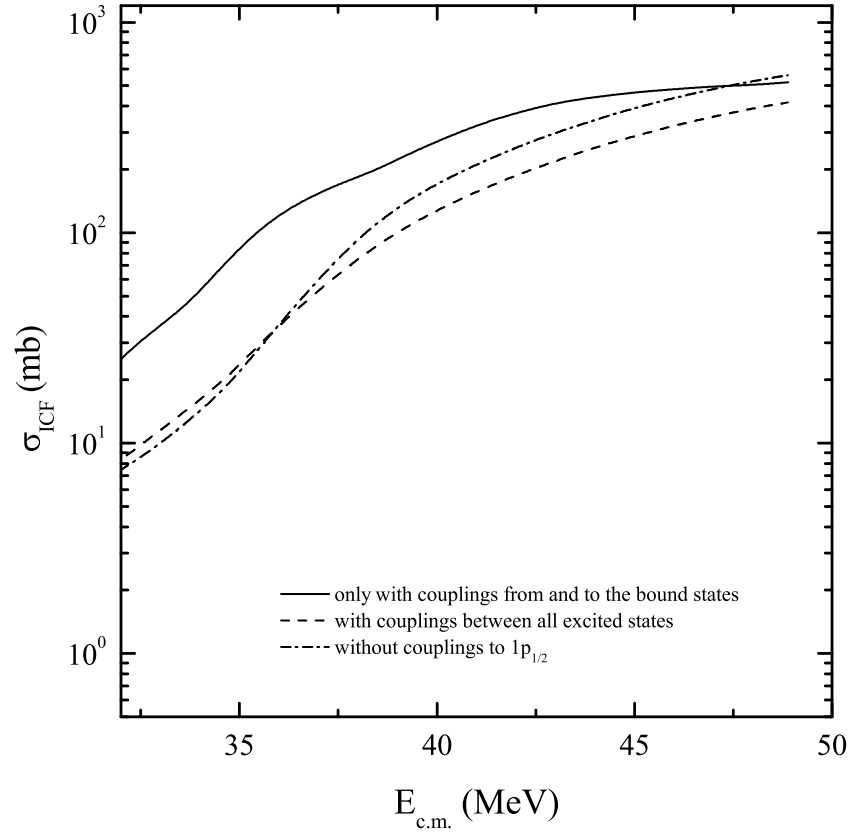


FIG. 3. Incomplete fusion excitation functions for both cases shown in Figs.2a (solid curve) and 2b (dashed curve). Incomplete fusion excitation function for the case of Fig.2b, but couplings to the ^{11}Be bound excited state $1p_{1/2}$ are not included (dot-dashed curve).

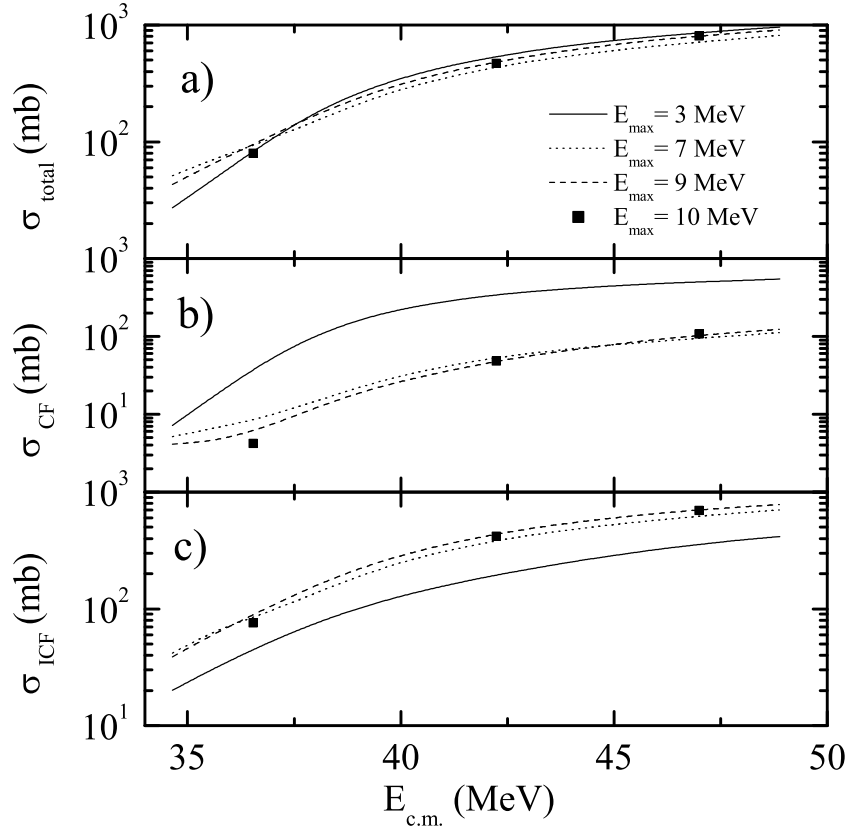


FIG. 4. Convergence of total (a), complete (b) and incomplete (c) fusion excitation functions for $^{11}\text{Be} + ^{208}\text{Pb}$ with regard to the maximum energy of the ^{11}Be continuum states included in the calculation. The s -, p - and d -wave continuum states for a density of the continuum discretisation of 2 bins/MeV, potential multipoles $K \leq 2$ and couplings between ^{11}Be excited states are included in the calculation. See text for further details.

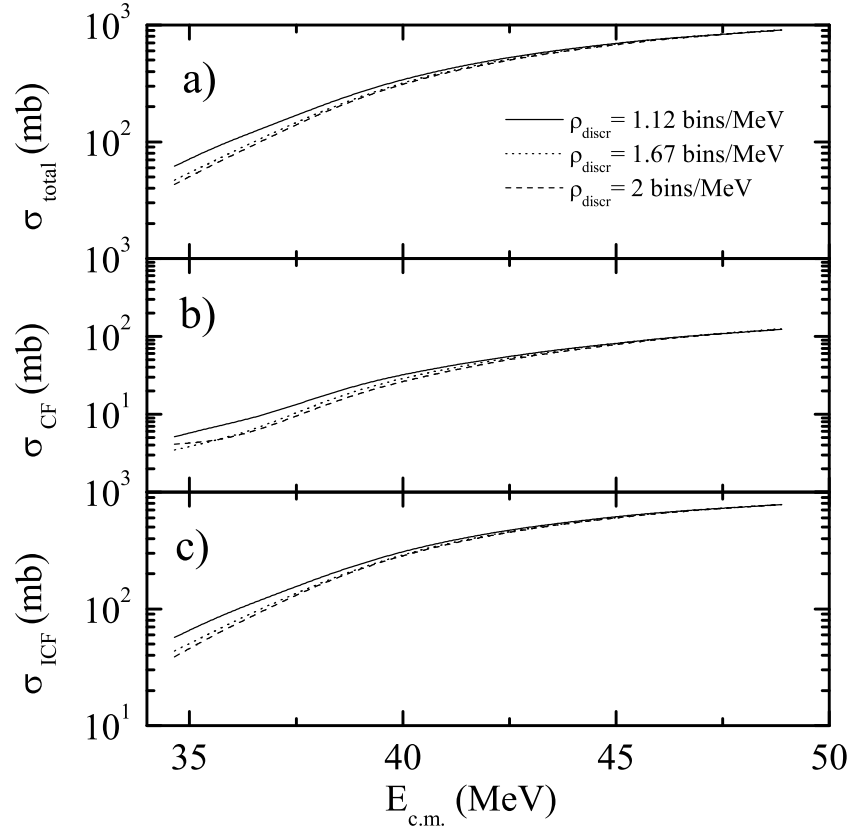


FIG. 5. The same as in Fig.4, but with regard to the density of the continuum discretisation. The maximum energy of the ^{11}Be continuum states is 9 MeV.

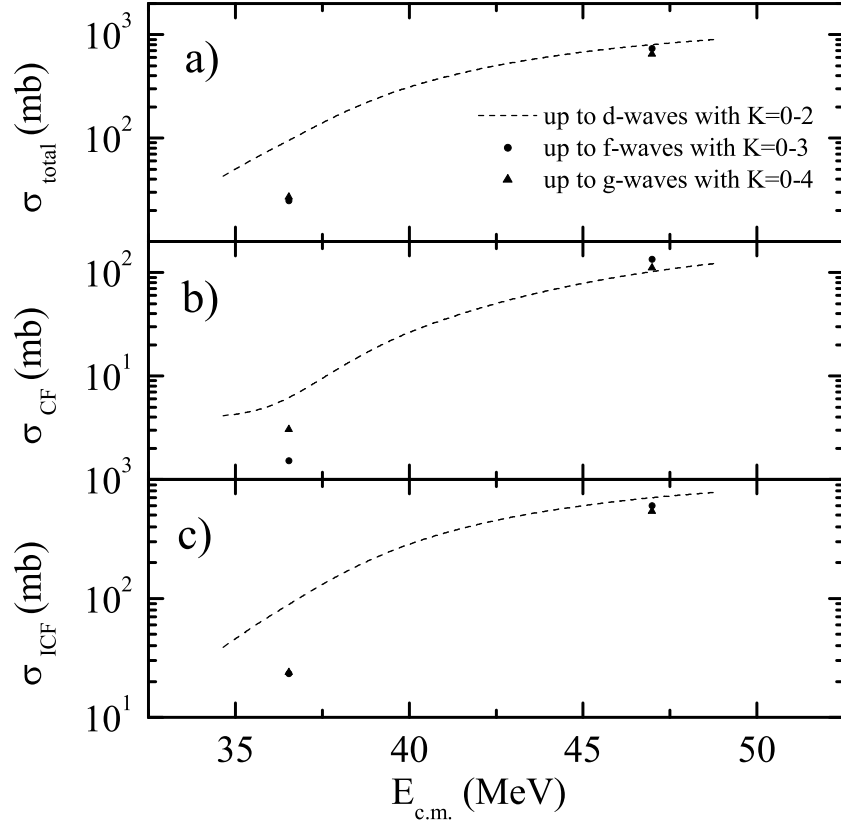


FIG. 6. The same as in Figs.4 and 5, but with regard to the number of partial waves in the continuum and potential multipoles. The maximum energy of the ^{11}Be continuum states and the density of the continuum discretisation are 9 MeV and 2 bins/MeV, respectively.

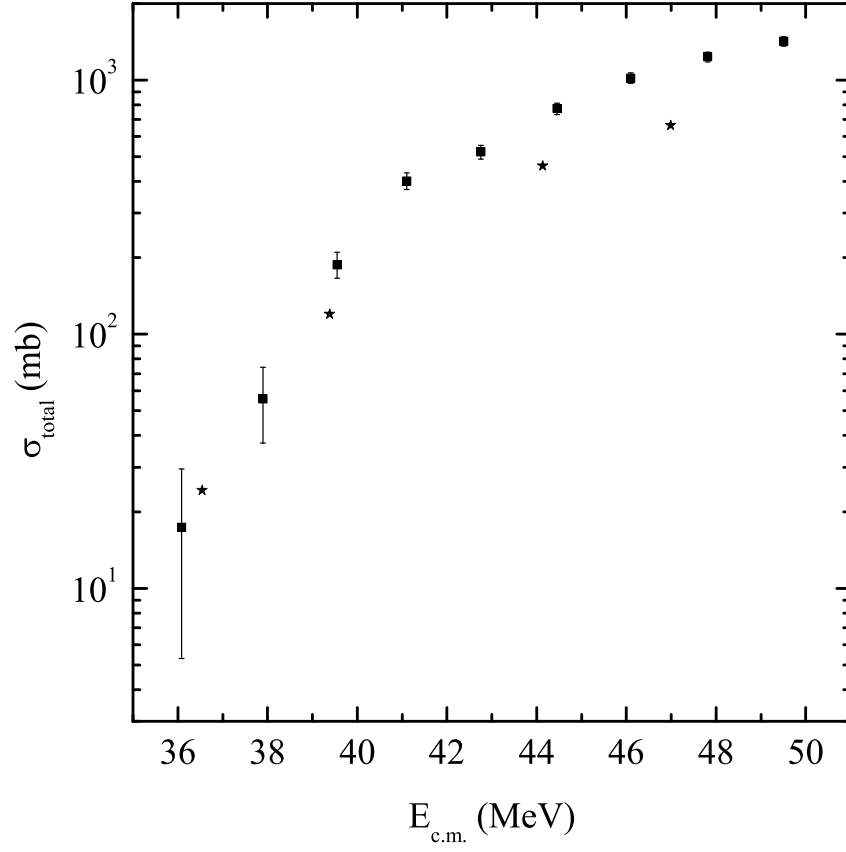


FIG. 7. Converged total fusion cross sections for $^{11}\text{Be} + ^{208}\text{Pb}$ (full stars) are compared with the experimental ones [10] for $^{11}\text{Be} + ^{209}\text{Bi}$ (full squares). A maximum energy of the ^{11}Be continuum states of 10 MeV, continuum partial waves up to g -waves for a density of the continuum discretisation of 2 bins/MeV, potential multipoles $K \leq 4$ and couplings between ^{11}Be excited states are included in the calculation.